



Evaluating the performance of *p*-type organic field-effect transistor using different source–drain electrodes

Mona Azimi, Jiaxin Fan, and Fabio Cicoira , Department of Chemical Engineering, Polytechnique Montréal, Montreal, QC H3T 1J4, Canada

Address all correspondence to Fabio Cicoira at fabio.cicoira@polymtl.ca

(Received 9 January 2024; accepted 4 March 2024; published online: 20 March 2024)

Abstract

We present our findings on organic field-effect transistors (OFETs) that utilize the conjugated copolymer poly[4-(4,4-dihexadecyl-4H-cyclopenta[1,2-b:5,4-b']-dithiophen-2-yl)alt[1,2,5]thiadiazolo[3,4-c]pyridine] as the active material, with electrodes composed of arrays of carbon nanotubes (CNTs). We employed three types of source and drain electrodes: gold, titanium, and CNT array electrodes with titanium contact pads. A comparison of characteristics of OFETs using these three different electrodes revealed the effectiveness of CNTs in enhancing charge carrier injection for OFETs. The OFETs based on CNT electrodes showed a twofold increase in the drain current and a threefold increase in charge carrier mobility compared to those with gold electrodes.

Introduction

Organic field-effect transistors (OFETs) are electronic devices with numerous potential applications, such as displays, chemical and mechanical sensors, and memory devices.^[1] OFETs are three-terminal devices, where the current flowing within the organic semiconductor channel between the source and drain can be modulated by the gate electric field. To achieve high-performance OFETs, many design parameters should be considered. Among these factors, the organic semiconductor/metal interfaces play a critical role, which strongly affects the effectiveness of charge injection. The charge carrier injection process from the metal contacts into the channel material is significantly influenced by the charge injection barriers. The charge injection barrier is defined as the energy difference between the Fermi level of the metal and the highest occupied molecular orbital (HOMO) in the case of hole injection in *p*-type semiconductors or the lowest unoccupied molecular orbital (LUMO) in the case of electron injection in *n*-type semiconductors within the organic layer. These barriers are determined by various factors, including geometrical considerations and the presence of trapping sites, primarily at the interfaces between the active layer and the metal electrodes.^[2] The contacts between metal and semiconductor should ideally be ohmic to ensure proper device operation. However, they are usually non-ohmic due to mismatch of HOMO or LUMO with the metal work function. As improving the charge injection is of utmost importance for OFETs, several approaches have been utilized to enhance the charge injection capability of OFETs, such as surface modification of electrodes via self-assembled monolayers (SAM),^[3,4] chemical doping of semiconductors,^[5] utilization of metal oxide insertion layer,^[6] and contact engineering through nanostructured electrodes with high porosity and roughness.^[7]

Substituting metallic electrodes with carbon-based electrodes, such as graphene and carbon nanotubes (CNTs), presents another viable option for optimizing charge carrier injection in OFETs. CNTs benefit from high carrier mobility and solution processability as well as good chemical and mechanical properties for the fabrication of flexible devices.^[8–10] CNT electrodes have been exploited in different organic electronic devices, such as solar cells, organic light-emitting diodes (OLEDs), and supercapacitors.^[11,12] Extremely large length to diameter ratio of CNT (one-dimensional structure) can cause the enhancement of the electric field at the nanotube–semiconductor interface, which helps charge injection by reducing the contact barrier.^[13] Enhanced electric field in the contact region of CNTs and organic semiconductors yields effective tunneling of charge carriers through the Schottky barrier at the interface. Devices based on arrays of CNT electrodes have been explored for different organic semiconductors, including small molecules and polymers, such as phenyl-C61-butyric acid methyl ester (PCBM),^[14] copper phthalocyanine,^[15] tetracyanoquinodimethane,^[16] as well as rubrene and its derivatives.^[17] CNT electrodes have been used in FETs based on inorganic metal oxides such as (a-IGZO).^[18] In addition, different configurations were demonstrated for CNT electrodes, including disordered arrays of nanotubes connecting metal pads to the organic semiconductor^[14–16] and dense CNT networks.^[19,20] In addition, CNTs with superior mechanical robustness and solution processability are suitable for flexible electronic device fabrications. Their solution processability allows for different fabrication techniques such as spray coating,^[21–23] inkjet printing,^[24] and screen printing.^[25]

In this work, we investigated the performance of OFETs based on the conjugated copolymer poly[4-(4,4-dihexadecyl-4H-cyclopenta[1,2-b:5,4-b']-dithiophen-2-yl)alt[1,2,5]

thiadiazolo[3,4-*c*]pyridine] (PCDTPT) with a bottom-gate bottom-contact configuration, using CNT electrodes as the source and drain electrodes. In our designed configuration, CNTs in the channel area were removed using photolithography and reactive ion etching (RIE) method, resulting in a unique configuration of CNT electrodes. In our work, a CNT network is formed, comprising bundles of CNTs that are in direct contact with the organic semiconductor. This configuration differs with the previous approach, where a disordered array of individual CNTs, commonly referred to as a “hairy” CNT electrode, is obtained by utilizing sonication to remove CNTs from the channel area.^[14,15] As a benchmark, we compared the performance of OFETs based on CNT electrodes with that of OFETs using gold (Au) electrodes as high work function metal and titanium (Ti) electrodes as low work function metal.

Results and discussion

PCDTPT is a donor–acceptor conjugated copolymer consisting of a cyclopenta[2,1-*b*:3,4-*b'*]dithiophene (CDT) donor unit and a^[1,2,5] thiadiazolo[3,4-*c*]pyridine (PT) acceptor unit, as illustrated in Fig. S1(a). The presence of strong electronic delocalization between these donor and acceptor units along the PCDTPT chain significantly enhances charge transport.

The carrier injection process, from the metal contact to the channel material, is determined by the charge injection barrier at the interfaces between the active layer and the metal electrodes. According to the Mott-Schottky model, the injection barrier is defined as the energy gap between the metal’s work function (Φ) and either the HOMO or the LUMO of the organic layer. Therefore, it is essential to consider the electronic properties and band alignment of the metal–semiconductor interfaces to understand the contact between the metal and semiconductor. The energy band diagram scheme depicting the HOMO–LUMO levels of PCDTPT, CNT, and the work functions of Au is presented in Fig. S1(b). The LUMO and HOMO levels of PCDTPT are measured at -3.65 eV and -5.81 eV, respectively.^[26]

The hole injection barrier (Φ_h) which is defined as the difference between the work function of metal contacts and HOMO level of *p*-type semiconductor is comparable for CNTs and Au.^[27,28] However, injection barrier is higher for Ti metal (with lower work function) compared to Au and CNT. Nanowires and nanotubes, owing to their one-dimensional structure, establish improved contact with organic semiconductors by concentrating field lines at the contact edges. This concentration of electric field lines results in a localized high electric field strength at the edge, which in turn can facilitate more efficient charge carrier injection.

We fabricated bottom-contact bottom-gate OFETs with CNT-based source and drain electrodes as depicted in Fig. S2 and explained in experimental section in detail. Concentric source and drain electrodes were used to eliminate the parasitic currents to easily compare the charge injection performance.

CNT electrodes have been utilized for OFETs as they showed better charge carrier injection, high mobility, and low contact resistance compared to Au electrodes.^[13–15] Here, we present a photolithography-assisted procedure for the fabrication of CNT electrodes, as illustrated in Fig. S2. To prepare CNT electrodes and prevent short circuits, it is essential to remove CNTs from the channel area. In prior studies involving OFETs with CNT electrodes,^[14–16] the sonication method was employed to eliminate CNTs from the channel area. This method resulted in individual CNTs or small bundles. In our current study, we adopted a different approach. We used photolithography to cover the CNTs near the metal contacts with photoresist and then employed RIE to selectively etch away the uncovered channel area. This method yields CNT electrodes with larger bundles compared to the previously used technique.

Figure 1 presents scanning electron microscopy (SEM) images of the CNT network deposition process on the Si/SiO₂ substrate at various stages of the process. In Fig. 1(a), the SEM illustrates the CNT network on the Si/SiO₂ substrate before heat treatment. It is noteworthy that Fig. 1(a) reveals the residual cellulose membrane, which remains discernible even after immersion in acetone during the procedure of transferring CNTs from membrane to silicon substrate (see experimental section for detailed information). We found that heating is an effective method to remove the cellulose membrane residue, which can be observed in the SEM image of the post-heat treatment CNT network [Fig. 1(b)] with a substantial reduction in membrane residues. Figure 1(c) depicts SEM images of the CNTs with patterned Ti metal contacts, and the CNTs situated between the metal contacts and also beneath the deposited metal contacts. Lastly, Fig. 1(d) illustrates the complete removal of CNTs within the channel region through a combination of photolithography and subsequent RIE processes.

Figure 2 displays the output characteristics (drain–source current (I_d) versus drain–source voltage (V_d)) for increasing values of gate–source voltage (V_g) for OFETs based on Au and CNT electrodes. Output curves of OFETs based on Ti electrode are shown in Fig. S3. *P*-type behavior is observed in all OFET devices, as expected [Fig. 2(a, b)]. The short-channel effect of CNT-based OFETs [Fig. 2(b)] may arise due to the configuration of CNT electrodes, wherein certain open ends of the CNTs are not only proximate to the metal contacts but also positioned a few microns distant from them. At low V_d values in the output curves, Au and Ti-based OFETs exhibit sublinear behavior [Figs. 2(c), S3(b)], whereas OFETs based on CNT electrodes demonstrate linear behavior [Fig. 2(d)]. This behavior is correlated with the better injection performance of CNT electrodes, while in Au and Ti-based OFETs, charge injection is hindered by injection barriers between the metal electrode and organic semiconductor. Comparing the saturated drain current in the output curves reveals that CNT OFETs achieve 100 times and 2 times higher drain current compared to Ti and Au electrodes, respectively. CNTs, due to their low dimensionality and high

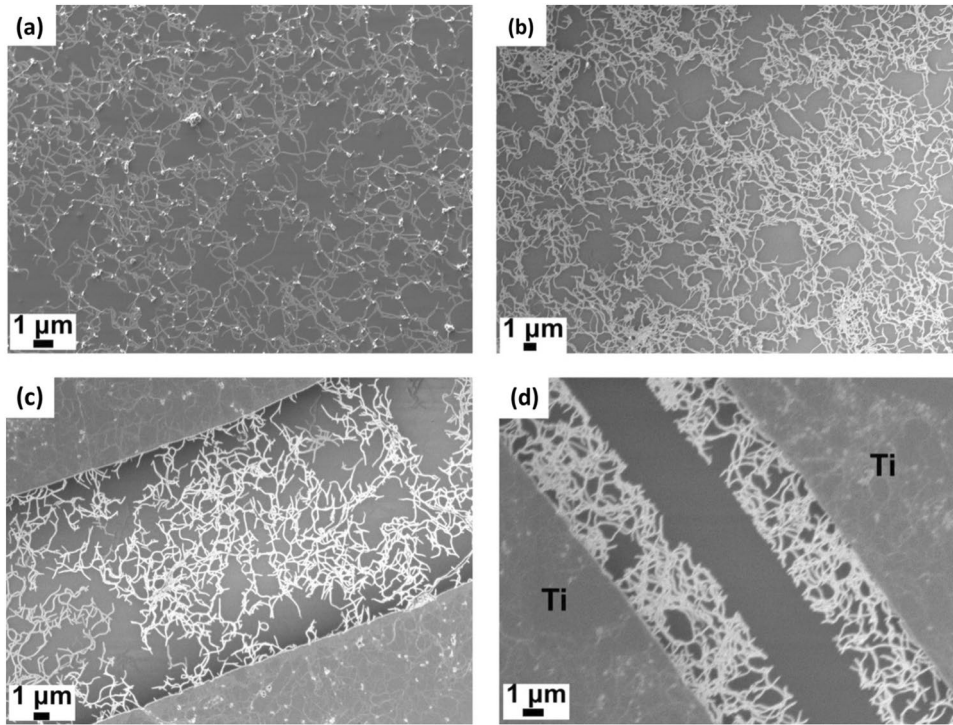


Figure 1. SEM images of deposited CNT networks on Si/SiO₂ substrates before heating at 350°C (a), and after heating (b). CNT network after deposition of metal contacts (c) and after second photolithography (d).

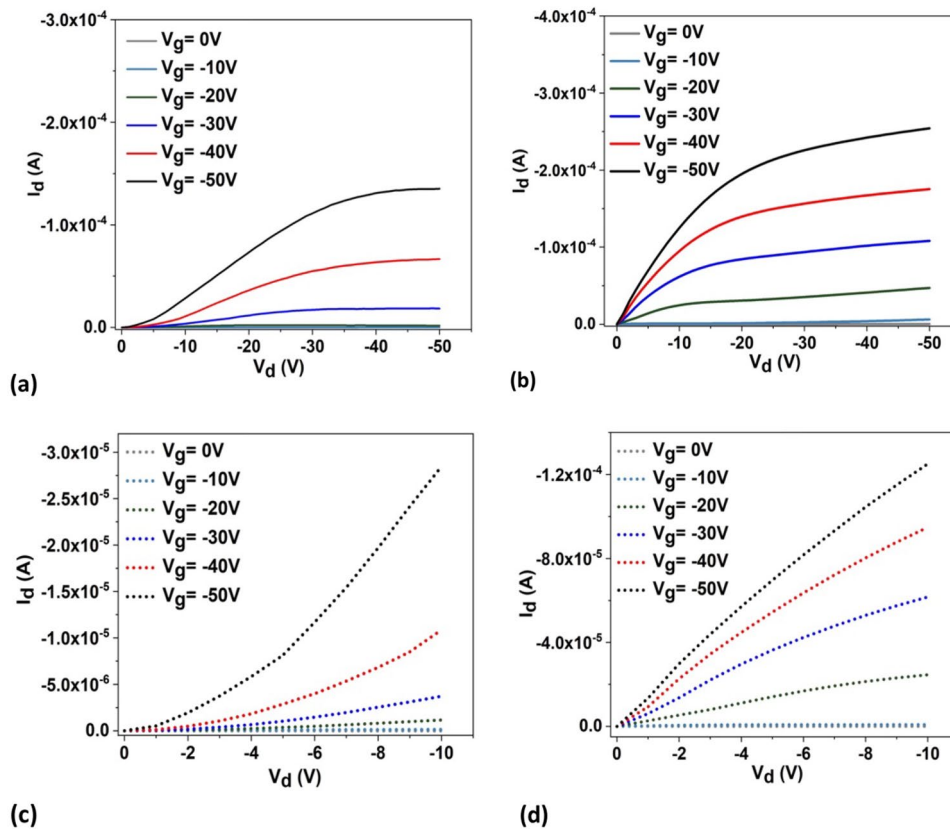


Figure 2. Output curves of OFETs based on Au (a), and CNT-based OFETs (b). Output curves in lower V_d range (< -10 V) for Au (c), and CNT-based OFETs (d).

aspect ratio, provide field enhancement tunneling and higher charge injection in the device.

Figure 3 illustrates the transfer characteristics, depicting drain–source current (I_d) against gate–source voltage (V_g), with V_d set at -50 V, for OFETs employing Au, and CNT electrodes. The transfer curve of OFET based on Ti electrode is depicted in Fig. S4. The key performance metrics of the OFETs are summarized in Table I. Values are averaged on three different electrodes of CNT and Au. The results for two other devices are shown in Figs. S5, S6. Hole mobility values were determined using the following equation:

$$I_d = \left(\frac{W}{L}\right)\mu C_i(V_g - V_{TH})V_d \quad (1)$$

where I_d is the drain current. W and L are the channel width and length, respectively. μ represents the carrier mobility. C_i is the capacitance of the dielectric layer. V_g , V_d , and V_{TH} are the gate, drain, and threshold voltages. Notably, the mobility of OFETs utilizing CNT electrodes is about three times higher than those with Au electrodes. The observed enhancement in mobility for these CNT electrodes is less significant compared to previously reported hairy CNT electrodes, which exhibited an order of magnitude increase in mobility when compared to Au electrodes.^[14,15] This phenomenon can likely be attributed to the nature of the hairy CNT electrodes, which comprise an array of individual CNTs without bundling, allowing the open ends of the CNTs to make direct contact with the semiconductor. In contrast, in etched CNT networks, we observed a higher prevalence of bundles in the region between the metal pads and the open ends of the CNTs. Consequently, in the latter case, only a limited number of open-ended, bundle-free CNTs contributed to the field-induced tunneling effect.

Conclusion

CNTs represent excellent electrode materials in the realm of organic electronics. An innovative and straightforward technique for fabricating CNT electrode arrays from a solution has been introduced and applied to investigate the impact of CNTs

Table I. Figure of merits for OFETs based on different electrodes.

Electrode material	Mobility ($\text{cm}^2/\text{V}\cdot\text{s}$)	On–Off ratio	Threshold voltage (V)
Au	0.08 ± 0.01	$\sim 10^7$	-2.6 ± 1.6
Ti	9.2×10^{-3}	$\sim 10^5$	-25
CNT	0.26 ± 0.04	$\sim 10^7$	-14.3 ± 1.5

Values are averaged on three different electrodes of CNT and Au.

in PCDTPT-based OFETs. Transistors utilizing CNT electrode arrays exhibited a moderate increase in the drain–source current and mobility values compared to the Au electrode. This method exemplifies its capability to deposit and pattern arrays of CNT electrodes, demonstrating its effectiveness in improving charge injection in OFETs. Incorporation of CNTs as electrodes for OFETs paves the way for fabrication of devices with high output current and mobility values. Also, using this method enables to make not only symmetric electrodes for transistor application but also asymmetric electrodes based on CNT in junction with other low work function metal contact for rectifying applications. Ongoing studies are dedicated to exploring the stability of OFETs based on CNT electrodes compared to those based on Au electrodes, and to elucidate the impact of enhanced electric fields on their stability.

Materials and methods

Single-wall carbon nanotubes (SWCNT) (RN220) were purchased from Nano Integris Co. and purified by chemical oxidation in concentrated nitric acid (HNO_3) prior to use, as reported elsewhere.^[29] An aqueous dispersion of CNT (1×10^{-3} mg/ml) with 2 wt% sodium cholate as a surfactant was prepared by sonication of CNTs in water using a tip horn sonicator for 10 min. One milliliter (1 mL) of SWCNT sodium cholate solution was diluted in 50 mL of water. A highly doped (p -type) silicon wafer with thermally evaporated SiO_2 (200 nm) was used as the substrate. The initial step involves depositing CNTs onto the membrane.

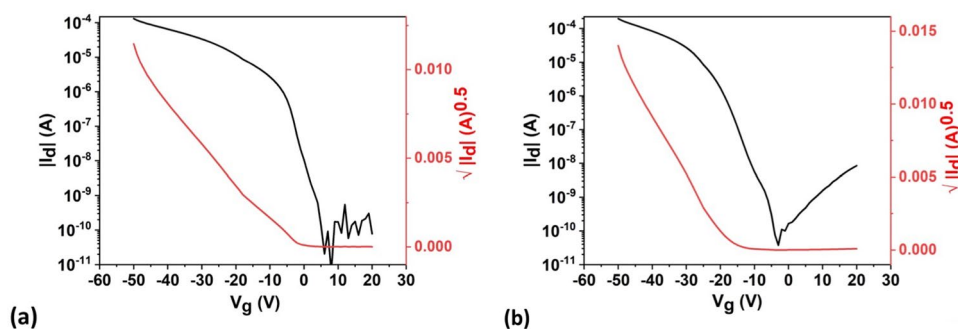


Figure 3. Transfer curves of OFETs based on Au (a), and CNT-based OFETs (b) at $V_d = -50$ V, right Y-axis corresponds to the square root of drain current.

To achieve this, a CNT dispersion was vacuum-filtered onto a hydrophilic mixed cellulose esters (MCE) membrane (MF-Millipore GSTF04700) resulting in the formation of a thin CNT layer on the membrane. To transfer the CNTs from the membrane onto the Si/SiO₂ substrates, the membranes were first immersed in dichlorobenzene and then laminated onto the Si/SiO₂ substrate by applying pressure to the membrane surface to adhere it on the substrate. The Si/SiO₂ substrates were transferred to a beaker containing acetone. The substrates were immersed in acetone for 6 days to dissolve the membrane on the Si/SiO₂ substrate. Finally, the substrates were rinsed with acetone, IPA, and water, followed by gentle drying with an N₂ flow.^[14] The Si/SiO₂ substrates with deposited CNTs were heated at 350°C for 3 h to ensure the removal of any residual membrane.

Source and drain electrodes of the transistor were patterned on the CNT-coated Si/SiO₂ substrate to obtain bottom-gate bottom-contact transistors. Prior to fabrication, the CNT-deposited substrates were dehydrated in an oven with an N₂ atmosphere to remove adsorbed water. Positive-tone photoresist (AZ900) was spin-coated onto the CNT-coated substrate at 3000 rpm for 1 min. After soft baking at 90°C for 90 s, the samples were exposed to UV light through a photomask using a Karl Suss mask aligner (MA-6). Next, the samples were baked at 115°C for 90 s and developed in AZ-726 (MicroChem) developer for 60 s. Finally, the samples were rinsed several times with deionized water to remove the developer residue and dried with an N₂ flow. To create contact pads for the CNT electrodes, a 40 nm-thick layer of titanium was deposited at a rate of 1 Å/s using an electron beam evaporator in a vacuum chamber, followed by a lift-off process with PG remover (MicroChem) at 50°C for 2 h.

The second photolithography process was performed using a second photomask and positive-tone photoresist (AZ900) to protect the CNTs in the vicinity of the metal pads. Oxygen reactive ion etching (150W, 2 min) was later applied to remove the uncovered CNTs, fabricating symmetric CNT electrodes. The samples were immersed in PG remover to strip out the photoresist, followed by rinsing with deionized water several times. The pre-patterned substrates were transferred into a glovebox (<5 ppm O₂, H₂O) for further fabrication and characterization of the transistor. The donor-acceptor conjugated copolymer (PCDTPT) was purchased from One-Material Co. and used as received. A solution of PCDTPT (2.5 mg/mL) was prepared in chloroform as the solvent and spin-coated onto the pre-patterned substrate at a speed of 1000 rpm for 1 min. The procedure for making CNT-based electrodes is depicted in Fig. S2. In addition, devices with Au and Ti metal electrodes, having the same channel length and width, were prepared to benchmark the CNT electrodes. The Au electrode was prepared by depositing a 5 nm Ti adhesion layer followed by 40 nm of gold, while the Ti electrode was prepared by depositing 40 nm of Ti metal. SEM images were obtained using a JEOL (JSM-7600TFE) instrument with a 1 keV accelerating voltage, 1 μA

emission current, and a 5 mm working distance. The Keysight B1500A semiconductor device parameter analyzer was used for characterizing the transistors.

Author contributions

MA: data collection and analysis; investigation; methodology; and writing original draft. JF: formal analysis; review and editing. FC: idea development; data organization; overseeing project logistics; managing resources; supervising; validating; writing, reviewing, and editing.

Funding

This work was supported by the Natural Sciences and Engineering Research Council of Canada (NSERC) through a Discovery Grant (RGPIN-2017-06319) and a Defense Research and Development Canada Grant (IDEaS Micronet CFPMN1-008) awarded to FC. MA is grateful for financial support from the Institut de l'Énergie Trottier for the PhD scholarship. JF acknowledges NSERC for a postdoctoral fellowship. This work was supported by CMC Microsystems through the MNT program.

Data availability

Data will be available upon request.

Declarations

Conflicts of interest

The authors declare that they have no conflict of interest.

Supplementary Information

The online version contains supplementary material available at <https://doi.org/10.1557/s43579-024-00539-2>.

References

1. K. Liu, B. Ouyang, X. Guo, Y. Guo, Y. Liu, Advances in flexible organic field-effect transistors and their applications for flexible electronics. *npj Flex. Electron.* **6**(1), 1 (2022)
2. C. Liu, Y. Xu, Y.Y. Noh, Contact engineering in organic field-effect transistors. *Mater. Today* **18**(2), 79 (2015)
3. T.K. Rockson, S. Baek, H. Jang, G. Choi, S. Oh, J. Kim, H. Cho, S.H. Kim, H.S. Lee, Engineering asymmetric charge injection/extraction to optimize organic transistor performances. *ACS Appl. Mater. Interfaces* **11**(10), 10108 (2019)
4. S. Casalini, C.A. Bortolotti, F. Leonardi, F. Biscarini, Self-assembled monolayers in organic electronics. *Chem. Soc. Rev.* **46**(1), 40 (2017)
5. X. Chen, X. Wei, H. Zhang, J. Wang, Highly improved charge injection in pentacene-based organic transistors by chemically doping with copper iodide interlayer. *Phys. Status Solid* **214**(8), 1700064 (2017)
6. K. Zhang, N.B. Kotadiya, X.Y. Wang, G.J.A. Wetzelaer, T. Marszalek, W. Pisula, P.W. Blom, Interlayers for improved hole injection in organic field-effect transistors. *Adv. Electron. Mater.* **6**(6), 1901352 (2020)

7. J. Li, Y. Hu, L. Yu, L. Li, D. Ji, L. Li, W. Hu, H. Fuchs, Recent advances of nanospheres lithography in organic electronics. *Small* **17**(28), 2100724 (2021)
8. H.T. Das, S. Dutta, T.E. Balaji, N. Das, P. Das, N. Dheer, R. Kanojia, P. Ahuja, S.K. Ujjain, Recent trends in carbon nanotube electrodes for flexible supercapacitors: a review of smart energy storage device assembly and performance. *Chemosensors* **10**(6), 223 (2022)
9. L. Qiu, M. Wang, T. Sun, Q. Lou, T. Chen, G. Yang, W. Qian, Z. Zhang, S. Yang, M. Zhang, An interfacial toughening strategy for high stability 2D/3D perovskite X-ray detectors with a carbon nanotube thin film electrode. *Nanoscale* **15**, 14574 (2023)
10. S.J. Lee, C.L. Kim, Highly flexible, stretchable, durable conductive electrode for human-body-attachable wearable sensor application. *Polym. Testing* **122**, 108018 (2023)
11. X. Shi, S. Chen, Carbon-based electrodes for organic solar cells. *ChemPlusChem* **2023**, e202300008 (2023)
12. P.H. Reddy, J. Amalraj, S. Ranganatha, S.S. Patil, S. Chandrasekaran, A review on effect of conducting polymers on carbon-based electrode materials for electrochemical supercapacitors. *Synth. Met.* **298**, 117447 (2023)
13. I. Valitova, M. Amato, F. Mahvash, G. Cantele, A. Maffucci, C. Santato, R. Martel, F. Cicoira, Carbon nanotube electrodes in organic transistors. *Nanoscale* **5**(11), 4638 (2013)
14. F. Cicoira, C.M. Aguirre, R. Martel, Making contacts to n-type organic transistors using carbon nanotube arrays. *ACS Nano* **5**(1), 283 (2011)
15. F. Cicoira, N. Coppedè, S. Iannotta, R. Martel, Ambipolar copper phthalocyanine transistors with carbon nanotube array electrodes. *Appl. Phys. Lett.* **98**(18), 87 (2011)
16. N. Coppedè, I. Valitova, F. Mahvash, G. Tarabella, P. Ranzieri, S. Iannotta, C. Santato, R. Martel, F. Cicoira, Titanyl phthalocyanine ambipolar thin film transistors making use of carbon nanotube electrodes. *Nanotechnology* **25**(48), 485703 (2014)
17. W. Xie, P.L. Prabhuramirashi, Y. Nakayama, K.A. McGarry, M.L. Geier, Y. Uragami, K. Mase, C.J. Douglas, H. Ishii, M.C. Hersam, Utilizing carbon nanotube electrodes to improve charge injection and transport in bis(trifluoromethyl)-dimethyl-rubrene ambipolar single crystal transistors. *ACS Nano* **7**(11), 10245 (2013)
18. R. Nirosha, R. Agarwal, Study of contact resistance in amorphous zinc oxide based thin-film transistors, in *2022 IEEE 3rd Global Conference for Advancement in Technology (GCAT)*. (IEEE, New York, 2022), p.1
19. B.K. Sarker, N. Kang, S.I. Khondaker, High performance semiconducting enriched carbon nanotube thin film transistors using metallic carbon nanotubes as electrodes. *Nanoscale* **6**(9), 4896 (2014)
20. M. Held, P. Laiho, A. Kaskela, F. Gannott, M. Rother, E. Kauppinen, J. Zaumseil, Dense carbon nanotube films as transparent electrodes in low-voltage polymer and all-carbon transistors. *Adv. Electron. Mater.* **4**(10), 1700331 (2018)
21. S. Vasquez, M.A.C. Angeli, M. Petrelli, M. Ahmad, B. Shkodra, B. Saloni-kidou, R.A. Sporea, A. Rivadeneyra, P. Lugli, L. Petti, Comparison of printing techniques for the fabrication of flexible carbon nanotube-based ammonia chemiresistive gas sensors. *Flex. Print. Electron.* **8**(3), 035012 (2023)
22. M. Abbaspour, B. Pourabbas, M. Azimi, G. Abdeali, A. Asgari, Solid-state supercapacitor based on breath figured polymethyl methacrylate deposited by graphene: the effect of electrode surface. *J. Mater. Sci. Mater. Electron.* **28**, 14121 (2017)
23. M. Azimi, M. Abbaspour, A. Fazli, H. Setoodeh, B. Pourabbas, Investigation on electrochemical properties of polythiophene nanocomposite with graphite derivatives as supercapacitor material on breath figure-decorated PMMA electrode. *J. Electron. Mater.* **47**, 2093 (2018)
24. S. Park, M. Shin, H. Kang, Y. Lee, Massive fabrication of carbon nanotube transistors by surface tension-driven inkjet-printing method, in *2023 IEEE International Conference on Flexible and Printable Sensors and Systems (FLEPS)*. (IEEE, New York, 2023), p.1
25. Y. Hua, M. Guan, L. Xia, Y. Chen, J. Mai, C. Zhao, C. Liao, Highly stretchable and robust electrochemical sensor based on 3D graphene oxide-CNT composite for detecting ammonium in sweat. *Biosensors* **13**(3), 409 (2023)
26. S. Song, S. Park, S. Kwon, B.H. Lee, J.A. Kim, S.H. Park, Y. Jin, J. Lee, I. Kim, K. Lee, Synthesis and characterization of phenanthrothiadiazole-based conjugated polymer for photovoltaic device. *Synth. Met.* **162**(21–22), 1936 (2012)
27. C. Li, F. Pan, X. Wang, L. Wang, H. Wang, H. Wang, D. Yan, Effect of the work function of gate electrode on hysteresis characteristics of organic thin-film transistors with Ta2O5/polymer as gate insulator. *Org. Electron.* **10**(5), 948 (2009)
28. M. Shiraishi, M. Ata, Work function of carbon nanotubes. *Carbon* **39**(12), 1913 (2001)
29. P. Gagnon, F. Lapointe, P. Desjardins, R. Martel, Double-walled carbon nanotube film as the active electrode in an electro-optical modulator for the mid-infrared and terahertz regions. *J. Appl. Phys.* **128**(23), 233103 (2020)

Publisher's Note Springer Nature remains neutral with regard to jurisdictional claims in published maps and institutional affiliations.

Springer Nature or its licensor (e.g. a society or other partner) holds exclusive rights to this article under a publishing agreement with the author(s) or other rightsholder(s); author self-archiving of the accepted manuscript version of this article is solely governed by the terms of such publishing agreement and applicable law.